

Photometric Properties of Jupiter Trojans detected by the Dark Energy Survey

1 JIANG PAN (潘嘉明) ^{1,2} HSING WEN LIN (林省文) ² DAVID W. GERDES ^{1,2} KEVIN J. NAPIER ²
2 JICHI WANG (王骥驰) ² T. M. C. ABBOTT,³ M. AGUENA,⁴ S. ALLAM ^{5,*} O. ALVES,^{6,4} D. BACON,⁷
3 P. H. BERNARDINELLI ⁸ G. M. BERNSTEIN ⁹ E. BERTIN,^{10,11} D. BROOKS ¹² D. L. BURKE,^{13,14}
4 A. CARNERO ROSELL ^{15,4,16} M. CARRASCO KIND ^{17,18} J. CARRETERO ¹⁹ M. COSTANZI,^{20,21,22} L. N. DA COSTA,⁴
5 M. E. S. PEREIRA,²³ J. DE VICENTE ²⁴ S. DESAI ²⁵ P. DOEL,¹² I. FERRERO,²⁶ D. FRIEDEL,¹⁷ J. FRIEMAN ^{5,27}
6 J. GARCÍA-BELLIDO ²⁸ M. GATTI,⁹ R. A. GRUENDL,^{17,18} J. GSCHWEND ^{4,29} K. HERNER ⁵ S. R. HINTON,³⁰
7 D. L. HOLLOWOOD,³¹ K. HONSCHIED ^{32,33} D. J. JAMES ³⁴ K. KUEHN ^{35,36} N. KUROPATKIN ⁵ M. MARCH,⁹
8 F. MENANTEAU ^{17,18} R. MIQUEL ^{37,19} F. PAZ-CHINCHÓN,^{17,38} A. PIERES ^{4,29} A. A. PLAZAS MALAGÓN ³⁹
9 M. RAVERI,⁹ M. RODRIGUEZ-MONROY,²⁴ A. K. ROMER ⁴⁰ E. SANCHEZ ²⁴ M. SCHUBNELL ⁶ I. SEVILLA-NOARBE ²⁴
10 M. SMITH ⁴¹ E. SUCHYTA ⁴² G. TARLE ⁶ D. TUCKER ⁵ A. R. WALKER ³ AND N. WEAVERDYCK^{6,43}

11 ¹Department of Astronomy, University of Michigan
12 Ann Arbor, 48109 MI, USA

13 ²Department of Physics, University of Michigan
14 Ann Arbor, MI 48109, USA

15 ³Cerro Tololo Inter-American Observatory, NSF's National Optical-Infrared Astronomy Research Laboratory, Casilla 603, La Serena,
16 Chile

17 ⁴Laboratório Interinstitucional de e-Astronomia - LIneA, Rua Gal. José Cristino 77, Rio de Janeiro, RJ - 20921-400, Brazil

18 ⁵Fermi National Accelerator Laboratory, P. O. Box 500, Batavia, IL 60510, USA

19 ⁶Department of Physics, University of Michigan, Ann Arbor, MI 48109, USA

20 ⁷Institute of Cosmology and Gravitation, University of Portsmouth, Portsmouth, PO1 3FX, UK

21 ⁸Astronomy Department, University of Washington, Box 351580, Seattle, WA 98195, USA

22 ⁹Department of Physics and Astronomy, University of Pennsylvania, Philadelphia, PA 19104, USA

23 ¹⁰CNRS, UMR 7095, Institut d'Astrophysique de Paris, F-75014, Paris, France

24 ¹¹Sorbonne Universités, UPMC Univ Paris 06, UMR 7095, Institut d'Astrophysique de Paris, F-75014, Paris, France

25 ¹²Department of Physics & Astronomy, University College London, Gower Street, London, WC1E 6BT, UK

26 ¹³Kavli Institute for Particle Astrophysics & Cosmology, P. O. Box 2450, Stanford University, Stanford, CA 94305, USA

27 ¹⁴SLAC National Accelerator Laboratory, Menlo Park, CA 94025, USA

28 ¹⁵Instituto de Astrofísica de Canarias, E-38205 La Laguna, Tenerife, Spain

29 ¹⁶Universidad de La Laguna, Dpto. Astrofísica, E-38206 La Laguna, Tenerife, Spain

30 ¹⁷Center for Astrophysical Surveys, National Center for Supercomputing Applications, 1205 West Clark St., Urbana, IL 61801, USA

31 ¹⁸Department of Astronomy, University of Illinois at Urbana-Champaign, 1002 W. Green Street, Urbana, IL 61801, USA

32 ¹⁹Institut de Física d'Altes Energies (IFAE), The Barcelona Institute of Science and Technology, Campus UAB, 08193 Bellaterra
33 (Barcelona) Spain

34 ²⁰Astronomy Unit, Department of Physics, University of Trieste, via Tiepolo 11, I-34131 Trieste, Italy

35 ²¹INAF-Osservatorio Astronomico di Trieste, via G. B. Tiepolo 11, I-34143 Trieste, Italy

36 ²²Institute for Fundamental Physics of the Universe, Via Beirut 2, 34014 Trieste, Italy

37 ²³Hamburger Sternwarte, Universität Hamburg, Gojenbergsweg 112, 21029 Hamburg, Germany

38 ²⁴Centro de Investigaciones Energéticas, Medioambientales y Tecnológicas (CIEMAT), Madrid, Spain

39 ²⁵Department of Physics, IIT Hyderabad, Kandi, Telangana 502285, India

40 ²⁶Institute of Theoretical Astrophysics, University of Oslo. P.O. Box 1029 Blindern, NO-0315 Oslo, Norway

41 ²⁷Kavli Institute for Cosmological Physics, University of Chicago, Chicago, IL 60637, USA

42 ²⁸Instituto de Física Teórica UAM/CSIC, Universidad Autónoma de Madrid, 28049 Madrid, Spain

43 ²⁹Observatório Nacional, Rua Gal. José Cristino 77, Rio de Janeiro, RJ - 20921-400, Brazil

44 ³⁰School of Mathematics and Physics, University of Queensland, Brisbane, QLD 4072, Australia

45 ³¹Santa Cruz Institute for Particle Physics, Santa Cruz, CA 95064, USA

46 ³²Center for Cosmology and Astro-Particle Physics, The Ohio State University, Columbus, OH 43210, USA

47 ³³Department of Physics, The Ohio State University, Columbus, OH 43210, USA

48 ³⁴Center for Astrophysics | Harvard & Smithsonian, 60 Garden Street, Cambridge, MA 02138, USA

49 ³⁵Australian Astronomical Optics, Macquarie University, North Ryde, NSW 2113, Australia

50 ³⁶Lowell Observatory, 1400 Mars Hill Rd, Flagstaff, AZ 86001, USA

51 ³⁷Institució Catalana de Recerca i Estudis Avançats, E-08010 Barcelona, Spain

³⁸*Institute of Astronomy, University of Cambridge, Madingley Road, Cambridge CB3 0HA, UK*

³⁹*Department of Astrophysical Sciences, Princeton University, Peyton Hall, Princeton, NJ 08544, USA*

⁴⁰*Department of Physics and Astronomy, Pevensey Building, University of Sussex, Brighton, BN1 9QH, UK*

⁴¹*School of Physics and Astronomy, University of Southampton, Southampton, SO17 1BJ, UK*

⁴²*Computer Science and Mathematics Division, Oak Ridge National Laboratory, Oak Ridge, TN 37831*

⁴³*Lawrence Berkeley National Laboratory, 1 Cyclotron Road, Berkeley, CA 94720, USA*

ABSTRACT

The Jupiter Trojans are a large group of asteroids that are co-orbiting with Jupiter near its L4 and L5 Lagrange points. The study of Jupiter Trojans is crucial for testing different models of planet formation that are directly related to our understanding of solar system evolution and formation. In this work, we select known Jupiter Trojans listed by the Minor Planet Center (MPC) from the full six years dataset (Y6) of the Dark Energy Survey (DES) to analyze their photometric properties. The DES data allow us to study Jupiter Trojans with a fainter magnitude limit than previous surveys in a homogeneous survey with *griz* band measurements. We extract a final catalog of 573 unique Jupiter Trojans. Of the extracted Jupiter Trojans, 547 belong to the L5 population, which has been less studied than Trojans in the L4 cloud. The color distribution of L5 Trojans is similar to that of L4 Trojans. We find that L5 Trojans' $g - i$ and $g - r$ colors become less red with fainter absolute magnitudes, a trend also seen in L4 Trojans. Both the L4 and L5 clouds consistently show such a color-size correlation over an absolute magnitude range $11 < H < 18$. We also use DES colors to perform taxonomic classifications. C and P-type asteroids outnumber D-type asteroids in the L5 Trojans DES sample, which have diameters in the 5 - 20 km range. This is consistent with the color-size correlation.

Keywords: Asteroids (72) — Jupiter trojans (874) — Trojan asteroids (1715)

1. INTRODUCTION

The properties of Jupiter Trojans, small bodies that populate the 1:1 mean motion resonance near Jupiter's L4 and L5 Lagrange points, encode important clues about the processes that shaped our solar system and its origins. Recent theories, e.g., the Nice Model (Morbidelli et al. 2005), Grand Tack (Walsh et al. 2011), and Jumping Jupiter (Nesvorný et al. 2013; Roig & Nesvorný 2015) support the idea that radial migrations have happened in the early solar system. Under this hypothesis, Jupiter Trojans reached their current orbits by scattering inward from the primordial planetesimal disk as the giant planets migrated outward. Thus, the Trojans may share the same origin as Kuiper belt objects in this scenario. The alternative hypothesis suggests that it is also possible for Jupiter Trojans to form in their current locations by capturing planetesimals during the formation of Jupiter (Marzari & Scholl 1998; Fleming & Hamilton 2000). Consequently, their relations with trans-Neptunian objects (TNOs) and other small-body populations, e.g., Hildas and main-belt asteroids (MBAs), contain crucial implications for the solar systems formation hypothesis (TNO: Fraser et al. 2014; Morbidelli et al. 2009, Hildas: Wong et al. 2017, MBAs: Yoshida et al. 2019). Over the last few decades, numerous observations, experiments, and analyses related to Jupiter Trojans have considerably deepened our understanding of their physical properties, including sizes, colors, and taxonomic types. However, our knowledge of the underlying mechanics and compositions responsible for those properties remains poorly constrained (Wong et al. 2019). With the upcoming exploration of Lucy spacecraft (Levison et al. 2021), further analysis of the Jupiter Trojans is an even more compelling task.

Jupiter Trojans have several important features. The color bimodality of Trojans has been claimed in many previous studies in both spectroscopic and photometric surveys (Szabó et al. 2007; Wong et al. 2014; Wong & Brown 2015). Szabó et al. (2007) analyzed 869 unique Jovian Trojans in the Sloan Digital Sky Survey Moving Object Catalogue third release. They found that the colors of Trojans have small scatters and are correlated with orbital inclination. Emery et al. (2011) identified two compositional groups in the Jovian Trojan population, which show the “red” and “less-red” spectrum. Wong & Brown (2015) found that the “red” and “less-red” groups show different magnitude distributions, with more “less red” Trojans in $g - i$ colors with decreasing sizes in the L4 clouds.

* Deceased.

Large-scale photometric surveys can statistically study the color and taxonomic type of Trojans, and these properties are indicators of the surface composition of Jupiter Trojans. Previously, the Sloan Digital Sky Survey (SDSS; Ivezić et al. 2001, 2002) and WISE (Mainzer et al. 2011) have studied surface properties for a large number of Jupiter Trojans. However, these surveys are generally biased toward Trojans with large sizes (usually bigger than diameters of 20 km). Suprime-Cam (SC) and Hyper Suprime-Cam (HSC), which are mounted on the 8-meter class Subaru telescope, have reached deeper magnitudes and have given insights into the magnitude distributions (Uehata et al. 2022; Yoshida & Terai 2017; Yoshida & Nakamura 2008, 2005) and color-magnitude relation of small Trojans (Wong & Brown 2015). However, those surveys generally lack the multiple band measurements that enable the measurement of taxonomic types.

This study, carried out with data from the Dark Energy Survey (DES) (DES Collaboration 2005) reaches a deeper magnitude limit, ~ 15 in absolute magnitude H_V and correspondingly to $m_V \sim 22$, than the 4th release of Sloan Digital Sky Survey Moving Object Catalogue (SDSS MOC-4; Ivezić et al. 2001, 2002). Also, DES photometry in the g , r , i , and z bands allows the classification of Trojans into different taxonomic types (e.g. Carvano et al. 2010; DeMeo & Carry 2013). The goal of this work is to extend our understanding of the Jupiter Trojans' physical properties at the diameters of 5 - 20 km (assuming a constant geometric albedo of 0.07 (Grav et al. 2011)) and use them to shed light on the formation and evolution of Trojans.

This paper presents the photometry of known Trojans from the MPC in the full six-year data set from DES. The number of identified L5 Jupiter Trojans is substantially higher than L4 Jupiter Trojans. We present the color distributions of Jupiter Trojans and compare them between L4 and L5 Trojans. We demonstrate the trend of L5 Trojans' absolute magnitudes with colors, and compared the color-size correlation in different surveys. Finally, we classify these Trojans into different taxonomic classes and further discuss the results' implications.

2. DES DATASET

The Dark Energy Survey (DES) (DES Collaboration 2005) was an optical survey carried out between 2013 and 2019 using the Dark Energy Camera (DECam, Flaugher et al. (2015)) on the 4-meter Blanco telescope at Cerro Tololo Inter-American Observatory in Chile. The DES consisted of two interleaved surveys: the wide survey, which imaged a 5000 sq. deg. area centered upon the north galactic cap in the $grizY$ bands to a single-exposure depth of $r \sim 23.8$, and the supernova survey (Bernstein et al. 2012), which imaged ten 3 sq. deg. DECam fields at approximately weekly intervals in the $griz$ bands. Though intended primarily as a cosmological survey, the DES's combination of a large survey area, multi-year time baseline, and single-exposure depth make it an outstanding tool for studying our solar system. DES has yielded discoveries of hundreds of new Kuiper Belt Objects (Bernardinelli et al. 2022, 2020; Khain et al. 2020), a dwarf planet candidate at 92 AU (Gerdes et al. 2017), several Neptune Trojans including the first ultra-red member of this population (Lin et al. 2019; Gerdes et al. 2016), and a giant Oort cloud comet (Bernardinelli et al. 2021). Despite the survey's success in discovering new outer Solar System objects, a search for new Jupiter Trojans is prohibitively expensive due to its computational complexity (Bernardinelli et al. 2022). Still, We were able to identify individual detections of known Trojans in the DES data (most Trojans have multiple individual detections).

The present work makes use of the single-exposure images and catalogs that comprise the DES Y6 data set. These images underlie the DES Gold v2.0 data set, whose coadd images and catalogs were publicly released in January 2021 as DES DR2 (Abbott et al. 2021). The dataset contains 107,631 single exposures. All $griz$ exposures are 90 s in duration. The ten 10 supernova fields are distributed within the footprint of DES and have longer exposures.

3. TROJANS IN THE DES DATA

This section describes how we extract known Jupiter Trojans listed in the Minor Planet Center (MPC) from the DES Y6 data and further clean the data to get a sample of Trojans with reliable photometry. As of 2021 September, the MPC lists 10,437 objects classified as Jupiter Trojans. First, we match exposure number and CCD in the DES Y6 data with the positions of known Trojans in this sample. Position uncertainties of identified object were estimated and set to be smaller than $2''$ in RA and DEC. Then, we obtain photometry of these identified objects from a catalog of sources detected in individual exposures in the DES Y6 data, excluding objects with nearby stationary objects. We derive absolute magnitudes H of these Trojans. Finally, we further constrain these objects in the number of single exposure and magnitude uncertainties to get a more reliable catalog of Trojans and photometry. Also, some objects listed as known Trojans are not long-term stable, and they are removed as described in Section 3.3 below.

3.1. Identifying Trojans in Y6 of data from DES

The Trojans in the MPC are complete to around absolute magnitude H of 14 on 2019 September 29 (Hendler & Malhotra 2020). Only DES Y6 exposures with ecliptic latitude from -30° to 30° are searched. We obtain the orbital elements of known Trojans from the MPC and use the SPACEROCKS package (Napier 2020) to propagate each Trojan to the epoch of each DES exposure. If the ephemeris position falls within the DECam field of view, the object is identified as a potential Trojan in the DES Y6 data. After this search, we obtain 13,732 exposures in DES Y6 data containing 1084 unique Trojans.

3.2. Photometry of Trojans

We cross-match these 1084 objects with sources detected in single exposures in the DES Y6 data with a separation smaller than $2''$. We exclude the source if there is a stationary object in coadded image catalogs within $1''$ in position to avoid the background contamination, so this reliably identifies moving objects uncontaminated by static sources (Bernardinelli et al. 2020). We also keep COADD objects with the `Nepoch` value, which is the number of single exposures comprising the coadded image, smaller or equal to 1 in all g , r , i , z , or Y -band. This means that they are moving objects, as their COADD objects are only composed of one single exposure measurement. Note that if an object has `Nepoch` values equal to zero in all bands, then the COADD object is also excluded as this means it is a faint object which falls below any single-exposure threshold and is only detectable in the coadd. At this stage, we reach 888 unique Trojans with 12,057 exposures.

Absolute magnitudes (H) of Trojans in each exposure are derived from apparent magnitude using the distances and phase angles at the epoch of exposure. The relation between apparent and absolute magnitude is:

$$m = H + 5 \log_{10}\left(\frac{r\Delta}{d_0^2}\right) - 2.5 \log_{10} q(\alpha), \quad (1)$$

where r and Δ are heliocentric and geocentric distance, respectively. The d_0 is 1 au, and $q(\alpha)$ is the phase integral. We chose the standard HG model with $G = 0.15$.

Once we derived the H for each object in each epoch in each band, the weighted means of H in each specific band are taken as the final value for absolute magnitude, which is:

$$H = \frac{\sum_{i=1}^n \frac{H_i}{\sigma_i^2}}{\sum_{i=1}^n \frac{1}{\sigma_i^2}}, \quad (2)$$

and the uncertainty is:

$$\sigma = \sqrt{\sigma_0^2 - \frac{2.5}{\ln(10)} \frac{\sigma_{flux}^2}{flux}}, \quad (3)$$

where the σ_0 is the value of zero point magnitude uncertainties and it is usually around 0.002 mag. The uncertainty for the absolute magnitudes of each Trojan in each band is:

$$\bar{\sigma} = \frac{1}{\sum_{i=1}^n \frac{1}{\sigma_i^2}}. \quad (4)$$

Note that we do not include uncertainty from rotation here since we do not have enough data on each Trojan to estimate it. We discuss of the effect of Trojan's rotations further in section 5.1.

3.3. Further constraints on the selected Trojans

There are uncertainties in the ephemeris positions which are not considered when deriving ephemeris positions in the process of identifying Trojans. We put constraints on the positional uncertainties to ensure that the selected objects are bona fide Trojans. The positional uncertainties are estimated using the JPL Horizons system. Uncertainties for every identified object at the time of its exposure time are estimated. The JPL Horizons system gives 3σ uncertainties around the nominal position in arcseconds. We constrain all Trojans to have positional uncertainties smaller than $2''$ in both RA and DEC. After this process, we arrive at 9864 individual detections of 775 unique Trojans.

To further improve the quality of our photometry, we require that the number of detections of each Trojan is larger than 1, and the magnitude uncertainty is smaller than 0.1. Moreover, the Trojans in MPC are selected automatically

Table 1. The final catalog of Jupiter Trojans in the six years dataset of DES

Column Name	Unit	Description
(1)	(2)	(3)
Name		MPC Designation
H_g	mag	Absolute magnitude in g band
σ_g	mag	Uncertainty in H_g
H_r	mag	Absolute magnitude in r band
σ_r	mag	Uncertainty in H_r
H_i	mag	Absolute magnitude in i band
σ_i	mag	Uncertainty in H_i
H_z	mag	Absolute magnitude in z band
σ_z	mag	Uncertainty in H_z
L_n		Assigned cloud (L4 or L5)

NOTE—The full version of this table is provided in a machine-readable format.

Table 2. Number of detected Jupiter Trojans in each band and cloud

Filter Band	L5	L4
g	429	14
r	272	14
i	320	21
z	328	18

188 using their orbital elements, which is not 100 percent reliable¹. We integrate all 584 objects to make sure that they
 189 have stable orbits like real Trojans. We find 11 objects that are not permanently in resonance out of 584 objects,
 190 indicating a $\sim 2\%$ contamination rate. We remove these eleven objects from the following analysis.

191 3.4. Final catalog of Trojans

192 Finally, we obtain a final catalog of Jupiter Trojans in the DES Y6 data, which contains 573 unique Trojans. In
 193 table 1, we present this catalog in a machine-readable format. Table 2 shows the number of detected Trojans in each
 194 band and cloud (L4 and L5). This corresponds to 178 L5 and 8 L4 unique Trojans with measurements in all bands.
 195 We present the analysis of this dataset in the Section 4.

196 Some Trojans are not assigned to a cloud by the MPC, probably due to delayed updates. We assign these Trojans
 197 to L4 if they are leading Jupiter by more than 20° and assign them to L5 if they are trailing Jupiter by 20° at the
 198 time of observation.

¹ <https://www.minorplanetcenter.net/iau/lists/Trojans.html>

4. RESULTS

In this section, we present the results from the photometry of Trojans in the DES data, including the absolute magnitude distribution, color-color diagram, and correlation between colors and sizes. We further investigate the color-size correlation in a combination of SDSS MOC-4, Subaru survey, and DES data. To help the comparison among different surveys, the g , r , i , and z -band DES photometric magnitudes were converted to SDSS photometric magnitudes using equations in Appendix A.4 of [Drlica-Wagner et al. \(2018\)](#) in the result section. Finally, we present the classification of taxonomic types for Trojans.

4.1. Color distributions of Jupiter Trojans

We show the color distribution of Jupiter Trojans in the diagonal of Fig. 1. The colors in $g-r$, $r-i$, and $i-z$ were restricted to -2 to 2 to eliminate unphysical red or blue colors. The histogram of colors does not show a bimodality even for bright objects, which has been discernible in the SDSS-MOC 4 data according to [Wong & Brown \(2015\)](#). We used the unbinned top-hat Kernel Density Estimation method to fit the color distributions and still detect no obvious bimodality. Thus, the lack of bimodality is not an issue with the choice of binning. This could be caused by the smearing of colors due to rotations of Trojans, as was suggested to produce a similar effect in faint L4 Trojans detected by Subaru survey ([Wong & Brown 2015](#)). The standard deviation for $i-z$, $g-r$, and $r-i$ are 0.31, 0.18, and 0.16 respectively for L5 Trojans. Standard deviations of the color distributions are likely to be enlarged by ~ 0.1 mag due to the effects of the rotations of Trojans, which will later be shown in section. 5.1.

Fig. 1 lower triangle shows the $g-r/r-i$, $g-r/i-z$, and $r-i/i-z$ color-color diagrams of Trojans. The colors are calculated from absolute magnitudes. The color of the sun is overplotted for comparison ([Holmberg et al. 2006](#)). Most L5 Trojans are slightly redder than the sun in both color-magnitude diagrams. Our sample contains only a few L4 Trojans, and most of them have similar colors to L5 Trojans. The mean colors of L4 Trojans are 0.42, 0.25, and 0.18 for $g-r$, $r-i$, and $i-z$ colors respectively, while those for L5 Trojans are 0.56, 0.22, and 0.17 respectively. The difference in these mean colors between the L4 and L5 clouds does not exceed 0.5 mag. No obvious classifications of red and less-red objects can be found in the color-color diagram. All colors, including $g-r$, $g-i$, $r-i$, $z-g$, $z-r$, and $i-z$, of the L4 and L5 Trojans were compared using two-sample Kolmogorov-Smirnov (K-S) test. The smallest p -value is from the $i-z$ color, which is 0.095. In this paper, we adopt a p value > 0.01 for the null hypothesis to be retained. We, thus, cannot reject the possibility that L4 and L5 Trojans' colors are drawn from the same distribution.

4.2. Sizes and colors relation

Here, we use the absolute magnitude to characterize Trojan's size, and studied its relation with colors (Fig. 2). The mean colors of $g-i$, $g-r$, $i-z$, and $r-i$ are the average of each bin of 1 mag, with uncertainties estimated within the same bin. We estimate the uncertainty as the standard error of the mean with equal weights. The absolute magnitude of the r band for the mean colors is restricted to 11 - 15, beyond which there are only a few data, so we omit them in this case. In a linear fit, there is a clear trend of decreasing mean colors in $g-i$ and $g-r$ of L5 Trojans. The best-fitted lines for the $g-i$ and $g-r$ mean colors have slopes of -0.028 ± 0.001 and -0.023 ± 0.004 , respectively. In comparison, the slopes for the $i-z$ and $r-i$ mean colors are 0.005 ± 0.005 and 0.001 ± 0.001 respectively. As a result, the best-fitted lines for $g-i$ and $g-r$ colors are consistent with negative slopes; in contrast, the slopes for $i-z$ and $r-i$ were very close to zero. Such a trend does not disappear if the bin size is changed to 0.5 mag. Also, shifting the center of the bin up by 0.5 mag does not significantly change the trend. Furthermore, we used F-test to compare the significance of $y = a + bx$ model and $y = a$ model for the data. F-test suggested that there is a clear linear relationship, i.e. $y = a + bx$ model, for $g-i$ and $g-r$ colors with sizes, but not for $i-z$ and $r-i$ colors. This further confirms our findings of the color-size correlation. Here we adopt a p value to be < 0.1 to reject the null hypothesis of no linear relationship. The correlation breaks down when the magnitude is brighter than 10 because only two objects are in that magnitude range. Such correlations were discovered for the first time in the L5 cloud of Trojans. The $g-i$ colors correlation with sizes agrees with the finding in [Wong & Brown \(2015\)](#), which used only L4 Trojans for their analysis.

However, the DES Trojans were observed at different epochs; the effect of the rotations, which have a typical amplitude of 0.2 mags, may contribute to such a pattern. In Sec. 5.1 we use simple simulations to show that the negative slopes are still present even when uncertainties from rotations are included. Also, selection effects may create spurious slopes in $g-i$ and $g-r$ colors with sizes. In particular, a different S/N level in one of two filters could mimic a similar relationship in sizes and colors. For example, if g band has a worse S/N than r or i bands, then redder objects become too faint to be detected in the g band at the faint end of magnitudes. In this scenario, the absence

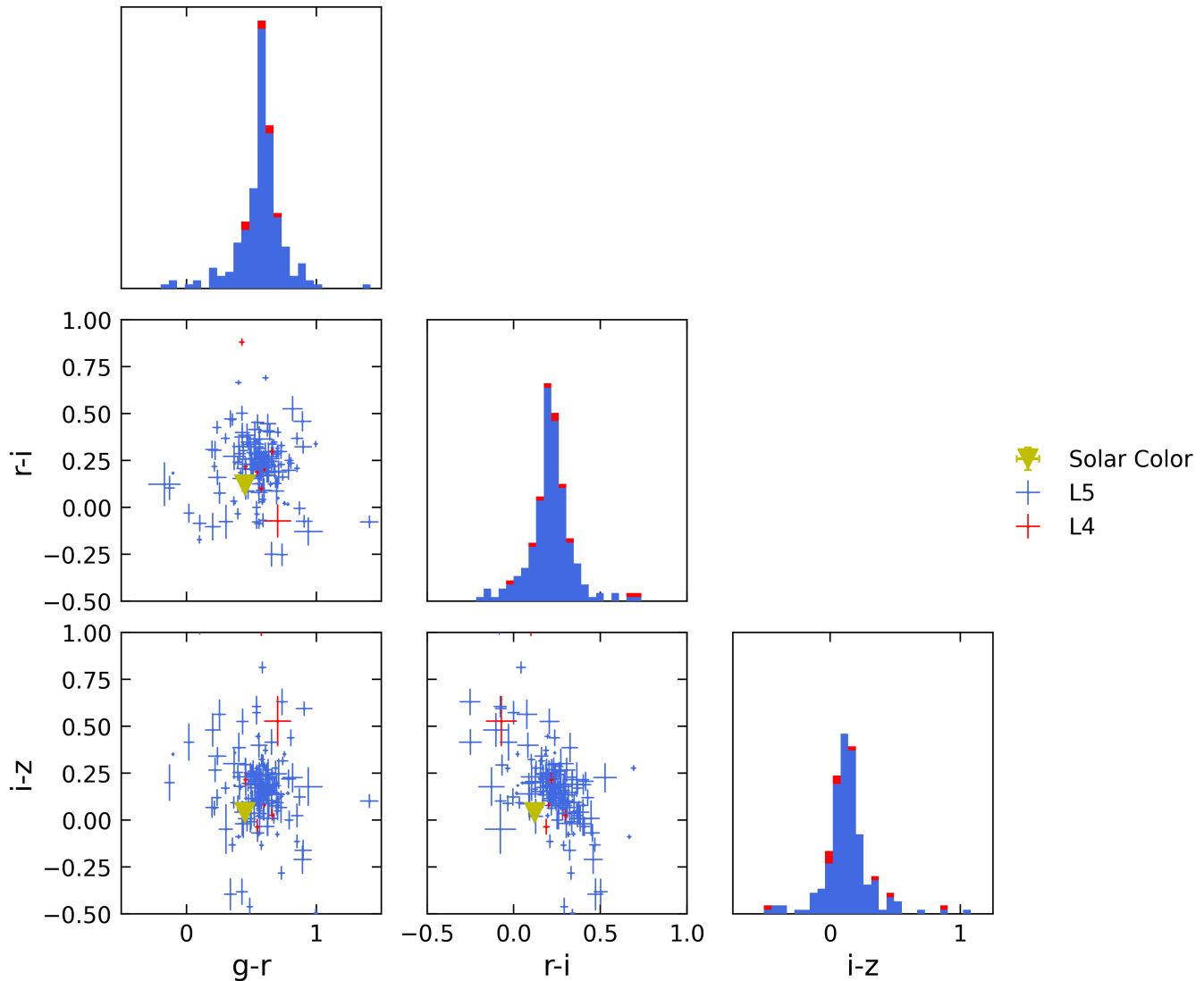


Figure 1. The lower triangle shows Jupiter Trojans’ colors for the L4 (red) and L5 clouds (blue). The diagonal plots show each color distribution in stacked histograms, with blue representing L5 cloud and red the L4 cloud. The yellow triangle shows the solar color. No bimodality has been found in the colors. L5 Trojans tend to be redder than the solar colors. Based on the K-S test, L4 and L5 Trojan’s colors distribution have no obvious differences.

249 of redder objects at the faint ends of the sample would lead to an artificial trend in $g - i$ and $g - r$ colors and sizes.
 250 To address this concern, we examine the S/N of Trojans at all filter bands around the magnitude limits. We found
 251 that at around S/N of 10 ($0.08 < \sigma_m < 0.14$, where σ_m is magnitude uncertainty) the magnitude median values are
 252 $g = 15.2$, $r = 14.5$, $i = 14.4$, and $z = 14.3$. This means that Trojans would have been more reliably detected in the
 253 g band than r or i bands, contrary to the potential problematic scenario. Therefore, the color-size correlations are
 254 unlikely to be caused by selection effects.

255 4.3. Comparison with Trojans in other surveys

256 We compared JTs in this study with Trojans in the SDSS MOC-4 and Wong & Brown (2015) (Fig. 3). We extracted
 257 known Trojans in the SDSS MOC-4 catalog. They lie in the regions with distances from 5.04 to 5.4 AU (DeMeo
 258 & Carry 2013) and have $e < 0.3$. The absolute magnitude was constrained to be brighter than 12.3, at which the
 259 SDSS MOC-4 catalog is almost complete. SDSS MOC-4 contains more Trojans than DES data due to the larger
 260 coverage area. Wong & Brown (2015) (hereafter Subaru data) used the Suprime-Cam instrument for the measurement
 261 of Trojan colors. The $g - i$ colors in their sample were already calibrated to the SDSS photometric system. We further

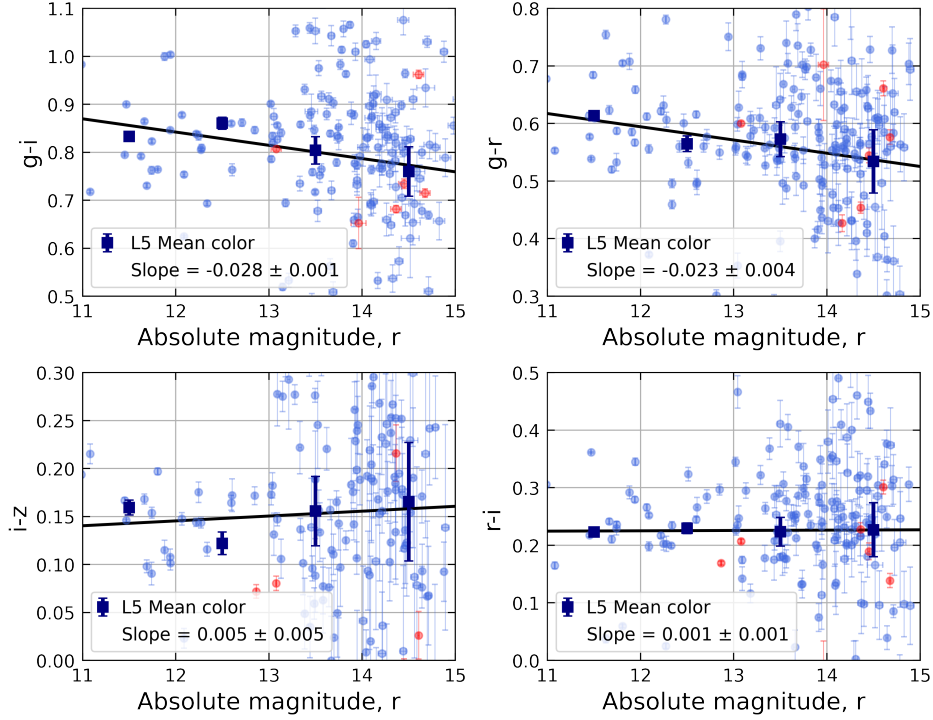


Figure 2. Color magnitude diagram of Trojans (red and blue dot for L5 and L4 Trojans respectively) and mean $g - i$, $g - r$, $i - z$, and $r - i$ colors of L5 Trojans after changing the size of bin to 1 mag (blue squares). The absolute magnitude is used to estimate the size of Trojans. The mean $g - i$ and $g - r$ colors show a trend of becoming less red with decreasing sizes of L5 Trojans. However, the mean $i - z$ and $r - i$ colors do not show such a trend. The black lines are the best-fitted straight lines, excluding outliers.

checked whether the conversion between SDSS and Suprime-Cam magnitudes depends on color, and found that the color-terms are almost negligible (see Appendix A). Thus, we take $g - i$ colors from Wong & Brown (2015) as SDSS $g - i$ colors. At the absolute magnitude interval from 11 to 13, where SDSS and DES data overlap, the mean $g - i$ color difference between SDSS and DES data is around 0.009 ± 0.04 mag. At absolute magnitude intervals from 13 to 15, the mean $g - i$ color between DES and Subaru data differs by around 0.03 ± 0.06 mag. The offsets between three different data sets are small compared with the dispersion of the data. However, there could still be contributions from some un-calibrated systematic effects other than color terms between the three photometric systems. Therefore, we conservatively shift the offsets, so that the overlapping absolute magnitude intervals of these three samples have the same mean $g - i$ colors. The following analyses would not be driven by the differences among the three photometric systems.

The left panel of Fig. 3 shows the histograms of L5 Trojans in the DES data, all the Trojans in the SDSS MOC-4 catalog, and L4 Trojans from Subaru data. The mean colors among the three datasets are very close, with a difference smaller than 0.1 mag. The small peak of DES L5 Trojans at $g - i$ around 1 mag is likely an artifact caused by the uncertainties in magnitudes, and it disappears at some other choices of binning. We also note that the DES Trojans colors have a larger scatter than SDSS and Subaru Trojans. We maintain that is an effect caused by the rotations of Trojans, and it will be discussed in section 5.1. Also, KS tests show that $g - i$ distributions in all three data are not compatible with each other.

Fig. 3 right panel shows the mean $g - i$ colors as a function of absolute magnitudes in the V band. The DES reaches a depth in between SDSS and Subaru. We found that the mean $g - i$ colors have a decreasing trend for SDSS, DES, and Subaru data. Mean $g - i$ colors and their uncertainties with a bin size of 1 mag are overplotted. The uncertainty is the standard error of the weighted mean with equal weights. Bright Trojans in the SDSS data seem to deviate from this trend ($H > 11$), as they tend to be bluer than the expected correlation. The agreement of these bright Trojans with the trend is sensitive to variations in bin sizes. It is likely that the strong color-size correlation breaks for these bright objects, consistent with finding in Szabó et al. (2007). Further studies are needed to understand why the

correlation breaks for these very big Trojans. The trend of objects at fainter magnitudes still shows a clear decreasing trend at different bin sizes. Regardless of the break at brighter magnitudes, the faint end of SDSS Trojans ($H > 11$) is still consistent with the expected color-size correlation. Also, the mean of the Trojan colors in the SDSS data is redder than both DES and Subaru data, with the mean colors in the Subaru data being the less-red. This is also consistent with the correlation. Additionally, we considered SDSS MOC-4 L4 and L5 clouds separately. No significantly different conclusions have been found.

A fitted line for the mean $g - i$ colors, shown as the red line in the right panel of Fig. 3, has a slope of -0.011 ± 0.001 . This slope is around three times smaller than the slope in the $g - i$ color in the DES data (-0.028 ± 0.001). Moreover, we performed a linear fit for L4 Trojans in the Subaru data only with absolute magnitude from 12 to 18 and $g - i$ color from 0.4 to 1.2 to exclude Trojans with color biases and large uncertainties (Wong & Brown 2015). Subaru L4 Trojans have a slope of -0.011 ± 0.002 . Similar to the joint data, the slope of Trojans in Subaru data is smaller than that of DES Trojans by around a factor of 3. Nevertheless, a negative slope is still statistically important in the Subaru data within the error bar. Also, both slopes in the red line of Fig. 3 right panel and Subaru data are within three sigma away from the DES derived slope. Here we only consider uncertainties in the colors. Thus, we found a similar relation between colors and sizes in DES and Subaru data. The strong correlation persists from faint Trojans (diameters $\lesssim 4$ km or $H \gtrsim 18$) until bright Trojans (diameters $\gtrsim 30$ km or $H \lesssim 11$). Even though we used L4 and L5 Trojans data, which have several differences in physical properties, the color-size correlation is present in both clouds with different magnitude ranges.

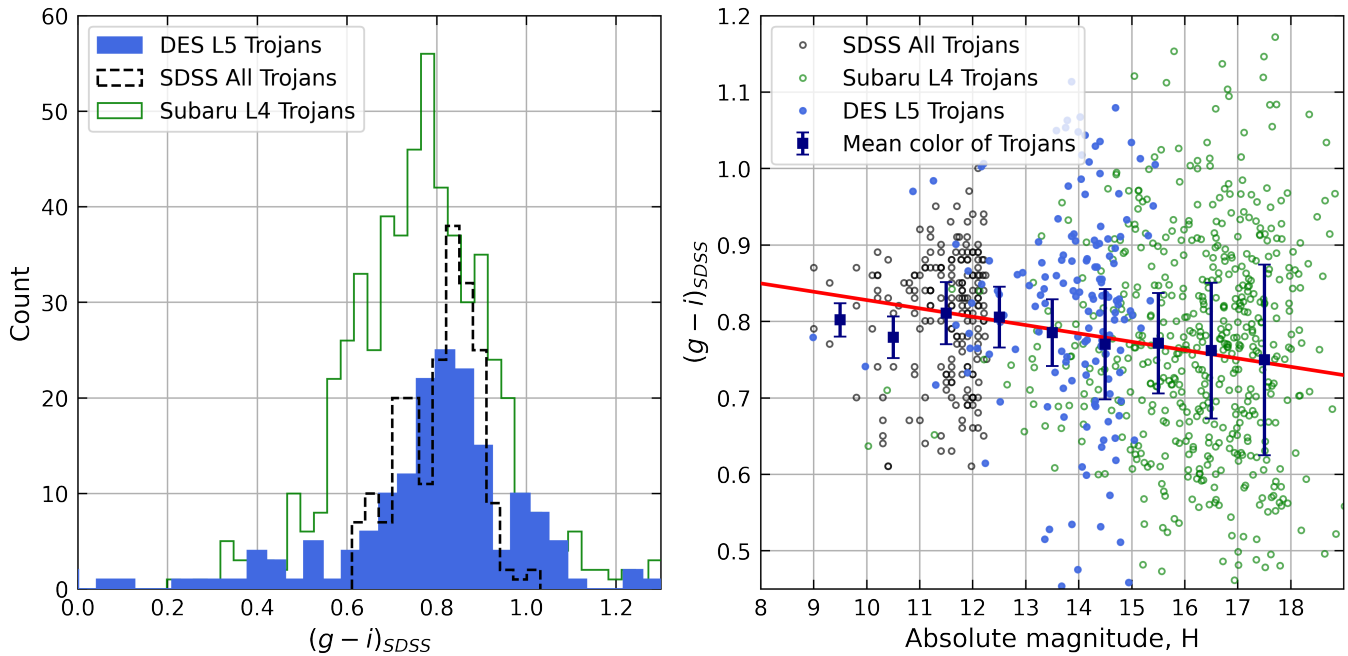


Figure 3. The left panel shows $g - i$ color distributions of Trojans in SDSS-MOC4 catalog, Subaru data, and known Trojans in DES data. DES g and i magnitudes were converted to SDSS magnitudes. The right panel shows the same data in a color absolute magnitude diagram, where the mean of $g - i$ colors in a bin size of 1 mag is overplotted. The mean $g - i$ colors show a trend of getting less-red with fainter magnitudes in DES and Subaru data.

4.4. Taxonomic classification of Jupiter Trojans

Generally, we expect the majority of Trojans to be D-type (red), P-type, or C-type (less-red) asteroids (DeMeo & Carry 2013). However, most of their classifications are based on Trojans in the SDSS and WISE data, which mostly have diameters > 20 km. The diameters of most Trojans in the DES data are smaller than that limit. This allows us to probe into the spectral types of a large sample of Trojans with diameters from 5 to 20 km.

In this section, we classify the detected Jupiter Trojans into different classes according to their colors following DeMeo & Carry 2013 classification, which used the spectral slope calculated from g , r , and i reflectance values (gri

311 slope) and $i - z$ colors. The DES photometric magnitudes have been converted to SDSS photometric magnitudes as
 312 described in section 4.3. Only Trojans with measurements in all $griz$ bands were classified, which include 178 L5
 313 Trojans and 8 L4 Trojans as mentioned in section 3.4.

314 Figure 4 shows the distribution of the 186 Trojans on gri slope vs $i - z$ diagram. The Trojans are mostly located
 315 in X and D-type regions, and the X-type region contains three degenerate classes E, M, and P. The large scattering
 316 is likely to be caused by the rotational effect (see section 5.1). The center of the distribution is located in the X-type
 317 region, which may indicate that in the range of $13 < H < 15$ or in a diameter size range of 5 to 13 km (assuming
 318 albedo = 0.07), there are more P-type Trojans than D-type. Such result is consistent with DeMeo & Carry 2014,
 319 which also shows that there are more P and C-type Trojans than D-type in the smaller size range. Since the P and
 320 C-type are less-red than the D-type (shallower gri slope), this result is consistent with what we found: the mean color
 321 is less-red for smaller size Trojans.

322 The amplitudes of asteroid rotations are generally around 0.2 mag (Mottola et al. 2011). Other than the color
 323 uncertainties from asteroid rotation, the intrinsic $i - z$ color uncertainties are usually around 0.04 mag. Figure 4
 324 include the intrinsic $i - z$ color uncertainties. Thus, Trojans with exotic taxonomic types, e.g., S and V-type, should
 325 be confirmed with further studies. The difference among C, X, and some D-type Trojans is very subtle, primarily
 326 dependent on the gri slope, as seen in Fig. 4. The uncertainties in slopes average on 2%.

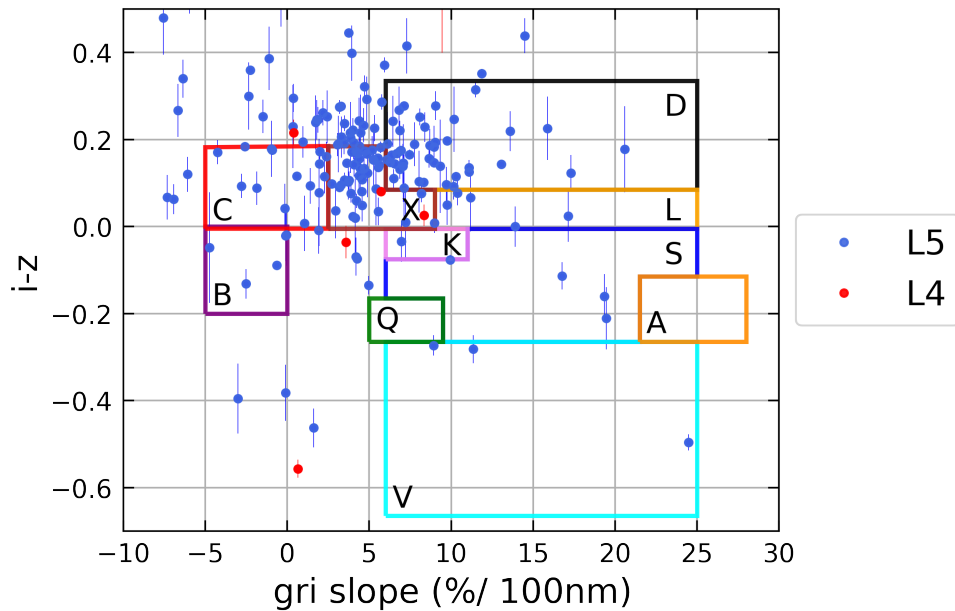


Figure 4. The classification of taxonomy for Jupiter Trojans. Each boundary represents a different class.

327 5. DISCUSSION

328 In this section, we discuss the effects of asteroid rotations on the color distributions and color-size correlations of
 329 DES Trojans and the implication for the formation and evolution of Trojans.

330 5.1. Effects of asteroid rotations

331 Since the DES color measurements of the Trojans were not simultaneous, the rotation of the objects needs to be
 332 taken into account. The DES measured colors can be described as the following equation:

$$333 C_{obs} = C_{true} + rot = \bar{C} + \sigma + rot, \quad (5)$$

334 here C_{obs} is the color we measured, C_{true} is the true color of the object, \bar{C} is the mean color of the sample, σ is
 335 the intrinsic color dispersion from the sample mean of the object, and rot is the rotational effect term, which is the

deviation induced by the object rotation. The mean colors we calculated in section 4.1 and 4.3 are:

$$\langle C_{obs} \rangle = \frac{1}{n} \sum_{i=1}^n (\bar{C} + \sigma_i + rot_i) = \bar{C} + \langle \sigma \rangle + \langle rot \rangle. \quad (6)$$

Here n is the total number of the sample. By definition, the average of intrinsic color dispersion term $\langle \sigma \rangle$ is zero. If the average of the rotational effect term $\langle rot \rangle$ is also zero, we have $\langle C_{obs} \rangle = \bar{C}$.

It is not possible to distinguish the σ and rot from the DES color measurements. Therefore, to test this assumption, we conservatively treated all of the deviations as intrinsic color dispersion and add the additional rotational term to each Trojan. Trojans at the sizes of DES generally have a light curve amplitude of 0.2 mag (Chang et al. 2021). We assumed that the light curves of Trojans follow a sinusoidal curve with amplitudes randomly drawn from a Gaussian distribution at a mean of 0.2 and a standard deviation of 0.1. We randomly sampled a phase of lightcurve from 0 to 2π for each observation and add this additional rotation term into the photometric measurements. Applying this step to all the objects, we obtained a new color distribution and a new mean color. After repeating the above steps 100,000 times, we found that the new mean colors agree with the original mean color within ± 0.017 .

Furthermore, we studied whether the observed decreasing trend of colors with fainter magnitudes is still present with the additional rotation term. We calculated the best-fitted slopes of mean $g-i$ colors vs. absolute magnitudes with a bin size of 1 mag. We found that the slopes tend to stay at a mean of -0.02 with a large standard deviation of 0.02. The negative slope is still present, and the additional rotation did not change the results. A larger standard deviation is expected as we added the extra deviations into the colors. From the above tests, we concluded that the average of rotation term $\langle rot \rangle$ is close to zero, and $\langle C_{obs} \rangle \sim \bar{C}$, which means the mean observed color is very close to the mean color of the Trojan sample.

The rotational effect also explains the larger color scattering in the DES data. As shown in Fig. 3, the DES L5 Trojans have $g-i$ colors have some extremes in both very red ($g-r > 1$) and very blue ($g-r < 0.6$) ends. In contrast, SDSS MOC-4 Trojans all lie in a very narrow range of colors. A simple explanation is that, unlike the DES data, SDSS colors were taken simultaneously, therefore, the scattering of SDSS colors is pure intrinsic color dispersion (σ). On the other hand, the scattering of DES colors is intrinsic color dispersion plus a rotational effect, as we described in Equation 5. To test this explanation, we ran two samples K-S test between the $g-i$ color dispersion distribution of the SDSS and DES samples and obtained a p-value of 0.004, which means the two $g-i$ color dispersion distributions are likely different from each other. This result was expected, because we compared the σ_{sdss} to the $\sigma_{DES} + rot_{DES}$. Then, we added the simulated rotational terms into the SDSS sample. The K-S test returned a p-value of 0.285, which means the color dispersion distributions were now indistinguishable. From the above test, we concluded that the larger color scattering in the DES data was likely induced by the rotational effect. The test also means that any other source of random additional photometric variance with similar uncertainties, e.g., different noise levels on observations of colors, is plausible to account for the difference between SDSS and DES colors.

We note that our function for the amplitudes is not perfect. Some Trojans do have light curve amplitudes larger than the 0.2 mag mean value that we have assumed above. Nevertheless, these larger light curve amplitudes are not common, as only $\sim 5\%$ of identified Trojans have amplitude larger than 0.4 mag (Mottola et al. 2011). We maintain that our approximation is sufficient for the analysis.

5.2. Color dichotomy and color-size correlation of Trojans

The fit of L5 Trojans mean $g-i$ colors in Fig. 3 is 0.84 mag at H of 9 mag and 0.74 mag at H of 18 mag. This agrees very well with the mean $g-i$ colors of the red (mean = 0.86 mag) and less-red (mean = 0.73 mag) populations in SDSS MOC-4 data, which are obtained by fitting a two-peaked Gaussian distribution by Wong & Brown (2015). The increasing fraction of P and C-type asteroids compared with D-type asteroids is also consistent with the increasing number of less-red objects; as P and C-type asteroids have smaller gri slopes than D-type asteroids. These two pieces of information hint strongly that two distinct populations with different size distributions and surface properties are responsible for the color bimodality of Trojans, with more P and C-type or less-red asteroids for smaller Trojans.

One hypothesis for the color-size correlation is that red populations were converted to the less-red population as they become fragments (Wong & Brown 2016), exposing fresher surfaces. They proposed that collisional fragments of both red and less-red groups become less-red in colors due to lack of CH_3OH and H_2S . However, further spectroscopic study has not identified any discernible feature in Jupiter Trojans (Wong et al. 2019). It is also possible that the color dichotomy is solely caused by the difference in surface properties between the two populations instead of a collisional

process. Since the two populations have different size distributions (Wong et al. 2014) and the less-red are more populated than the red group in the smaller end, the color-size correlation reported in Wong & Brown 2015 and this work would be an observational consequence of this fact. Nevertheless, whatever mechanisms created the color-size correlation of Jovian Trojans, it must be a general effect between L4 and L5, as both L4 and L5 Trojans share the same color-size trend. Finally, the color-size correlation was not obvious in the colors of $i - z$ and $r - i$ in the DES data compared with $g - i$ and $g - r$ colors. Both $i - z$ and $r - i$ colors were almost constant with magnitudes. This is consistent with the fact that the slope of the reflectance spectrum between the red and less-red groups tends to get closer in longer wavelength (Emery et al. 2011).

6. SUMMARY

We extracted known Jovian Trojans from the DES dataset using their orbital parameters in the MPC database. After excluding stationary objects, constraining uncertainties in the positions and photometry, and removing unstable asteroids, we reach a catalog of 547 unique L5 Trojans and 26 unique L4 Trojans. Using this sample, we study the color distributions of known Trojans in DES data and find no obvious differences in L4 and L5 Trojan color distributions. The color of $g - i$ and $g - r$ decreases with smaller sizes of the L5 Trojans, which is similar to the same color-size trend found in the L4 Trojans (Wong & Brown 2015). We find no obvious correlations between $r - i/i - z$ colors and size of L5 Trojans from the range of $11 < Hr < 15$. Joint the colors of DES Trojans with the SDSS MOC-4 data catalog and L4 Trojans from Wong & Brown (2015), we find strong evidence for the color-size correlation of Jovian Trojans, down to absolute magnitudes of 18. Finally, we classify taxonomic types of L5 Trojans and find more potential C and P-type (less-red colored) than D-type (red-colored) asteroids at diameters of 5 - 20 km. The increasing number of C and P-type Trojans is consistent with their color-size correlations, which show that more less-red colored Trojans are at the small-sized end.

Future surveys are needed to understand the physical properties and mechanics responsible for the correlations in taxonomic classes/colors and sizes of Jupiter Trojans. We expect that the Lucy mission will greatly enhance our knowledge of the composition of Jupiter Trojans.

This material is based upon work supported by the National Aeronautics and Space Administration under grant No. NNX17AF21G issued through the SSO Planetary Astronomy Program and by the National Science Foundation under grant No. AST-2009096. We thank Ian Wong and Michael E. Brown for sharing data of Trojans described in Wong & Brown (2015).

Funding for the DES Projects has been provided by the U.S. Department of Energy, the U.S. National Science Foundation, the Ministry of Science and Education of Spain, the Science and Technology Facilities Council of the United Kingdom, the Higher Education Funding Council for England, the National Center for Supercomputing Applications at the University of Illinois at Urbana-Champaign, the Kavli Institute of Cosmological Physics at the University of Chicago, the Center for Cosmology and Astro-Particle Physics at the Ohio State University, the Mitchell Institute for Fundamental Physics and Astronomy at Texas A&M University, Financiadora de Estudos e Projetos, Fundação Carlos Chagas Filho de Amparo à Pesquisa do Estado do Rio de Janeiro, Conselho Nacional de Desenvolvimento Científico e Tecnológico and the Ministério da Ciência, Tecnologia e Inovação, the Deutsche Forschungsgemeinschaft and the Collaborating Institutions in the Dark Energy Survey.

The Collaborating Institutions are Argonne National Laboratory, the University of California at Santa Cruz, the University of Cambridge, Centro de Investigaciones Energéticas, Medioambientales y Tecnológicas-Madrid, the University of Chicago, University College London, the DES-Brazil Consortium, the University of Edinburgh, the Eidgenössische Technische Hochschule (ETH) Zürich, Fermi National Accelerator Laboratory, the University of Illinois at Urbana-Champaign, the Institut de Ciències de l’Espai (IEEC/CSIC), the Institut de Física d’Altes Energies, Lawrence Berkeley National Laboratory, the Ludwig-Maximilians Universität München and the associated Excellence Cluster Universe, the University of Michigan, NSF’s NOIRLab, the University of Nottingham, The Ohio State University, the University of Pennsylvania, the University of Portsmouth, SLAC National Accelerator Laboratory, Stanford University, the University of Sussex, Texas A&M University, and the OzDES Membership Consortium.

Based in part on observations at Cerro Tololo Inter-American Observatory at NSF’s NOIRLab (NOIRLab Prop. ID 2012B-0001; PI: J. Frieman), which is managed by the Association of Universities for Research in Astronomy (AURA) under a cooperative agreement with the National Science Foundation.

The DES data management system is supported by the National Science Foundation under Grant Numbers AST-1138766 and AST-1536171. The DES participants from Spanish institutions are partially supported by MICINN under grants ESP2017-89838, PGC2018-094773, PGC2018-102021, SEV-2016-0588, SEV-2016-0597, and MDM-2015-0509, some of which include ERDF funds from the European Union. IFAE is partially funded by the CERCA program of the Generalitat de Catalunya. Research leading to these results has received funding from the European Research Council under the European Union’s Seventh Framework Program (FP7/2007-2013) including ERC grant agreements 240672, 291329, and 306478. We acknowledge support from the Brazilian Instituto Nacional de Ciência e Tecnologia (INCT) do e-Universo (CNPq grant 465376/2014-2).

This manuscript has been authored by Fermi Research Alliance, LLC under Contract No. DE-AC02-07CH11359 with the U.S. Department of Energy, Office of Science, Office of High Energy Physics.

Facilities: DECam

Software: Spaceroch (Napier 2020), Astropy (Astropy Collaboration et al. 2013, 2018), SciPy (Virtanen et al. 2020), Numpy (Harris et al. 2020), Matplotlib (Hunter 2007), Pandas (McKinney et al. 2010)

APPENDIX

A. COLOR CONVERSION BETWEEN SUBARU/SUPRIME-CAM AND SDSS PHOTOMETRIC SYSTEM

To convert from Subaru/Suprime-Cam g_{sc} , i_{sc} magnitudes to SDSS g_{sdss} , i_{sdss} , we evaluate the linear color conversions between the two systems using in-frame background stars matched in the SDSS DR12 catalogs. We select the SDSS sources with $g_{sdss} < 21$, $i_{sdss} < 21$, and $0 < (g - i)_{sdss} < 2.5$ to this evaluation. Then, we solve the following equation:

$$m_{sc} = m_{sdss} + C (g - i)_{sdss}. \quad (\text{A1})$$

Here m_{sc} and m_{sdss} are the Subaru and SDSS magnitude, respectively, and C is a linear color-term. By solving this equation using the in-frame SDSS sources, we find:

$$g_{sc} = g_{sdss} - 0.03(g - i)_{sdss}, \quad (\text{A2})$$

and

$$i_{sc} = i_{sdss} - 0.02(g - i)_{sdss}. \quad (\text{A3})$$

Combining Equation A2 and Equation A3, we have

$$(g - i)_{sc} = 0.99(g - i)_{sdss}. \quad (\text{A4})$$

Since the $g - i < 1$ for most of Trojans, the errors induced by color conversions between Subaru and SDSS photometry systems are less than 1%. Therefore, we conclude that the effect of color-term is negligible.

REFERENCES

- Abbott, T. M. C., Adamów, M., Agüena, M., et al. 2021, The Astrophysical Journal Supplement Series, 255, 20, doi: [10.3847/1538-4365/ac00b3](https://doi.org/10.3847/1538-4365/ac00b3)
- Astropy Collaboration, Robitaille, T. P., Tollerud, E. J., et al. 2013, A&A, 558, A33, doi: [10.1051/0004-6361/201322068](https://doi.org/10.1051/0004-6361/201322068)
- Astropy Collaboration, Price-Whelan, A. M., Sipőcz, B. M., et al. 2018, AJ, 156, 123, doi: [10.3847/1538-3881/aabc4f](https://doi.org/10.3847/1538-3881/aabc4f)
- Bernardinelli, P. H., Bernstein, G. M., Sako, M., et al. 2020, ApJS, 247, 32, doi: [10.3847/1538-4365/ab6bd8](https://doi.org/10.3847/1538-4365/ab6bd8)
- Bernardinelli, P. H., Bernstein, G. M., Montet, B. T., et al. 2021, ApJL, 921, L37, doi: [10.3847/2041-8213/ac32d3](https://doi.org/10.3847/2041-8213/ac32d3)
- Bernardinelli, P. H., Bernstein, G. M., Sako, M., et al. 2022, ApJS, 258, 41, doi: [10.3847/1538-4365/ac3914](https://doi.org/10.3847/1538-4365/ac3914)
- Bernstein, J. P., Kessler, R., Kuhlmann, S., et al. 2012, ApJ, 753, 152, doi: [10.1088/0004-637X/753/2/152](https://doi.org/10.1088/0004-637X/753/2/152)
- Carvano, J. M., Hasselmann, P. H., Lazzaro, D., & Mothé-Diniz, T. 2010, A&A, 510, A43, doi: [10.1051/0004-6361/200913322](https://doi.org/10.1051/0004-6361/200913322)
- Chang, C.-K., Chen, Y.-T., Fraser, W. C., et al. 2021, PSJ, 2, 191, doi: [10.3847/PSJ/ac13a4](https://doi.org/10.3847/PSJ/ac13a4)
- DeMeo, F. E., & Carry, B. 2013, Icarus, 226, 723, doi: [10.1016/j.icarus.2013.06.027](https://doi.org/10.1016/j.icarus.2013.06.027)
- . 2014, Nature, 505, 629, doi: [10.1038/nature12908](https://doi.org/10.1038/nature12908)
- DES Collaboration. 2005, ArXiv e-prints. <https://arxiv.org/abs/astro-ph/0510346>
- Drlica-Wagner, A., Sevilla-Noarbe, I., Rykoff, E. S., et al. 2018, ApJS, 235, 33, doi: [10.3847/1538-4365/aab4f5](https://doi.org/10.3847/1538-4365/aab4f5)
- Emery, J. P., Burr, D. M., & Cruikshank, D. P. 2011, AJ, 141, 25, doi: [10.1088/0004-6256/141/1/25](https://doi.org/10.1088/0004-6256/141/1/25)
- Flaugher, B., Diehl, H. T., Honscheid, K., et al. 2015, The Astronomical Journal, 150, 150. <https://arxiv.org/abs/1504.02900>
- Fleming, H. J., & Hamilton, D. P. 2000, Icarus, 148, 479, doi: [10.1006/icar.2000.6523](https://doi.org/10.1006/icar.2000.6523)
- Fraser, W. C., Brown, M. E., Morbidelli, A., Parker, A., & Batygin, K. 2014, ApJ, 782, 100, doi: [10.1088/0004-637X/782/2/100](https://doi.org/10.1088/0004-637X/782/2/100)
- Gerdes, D. W., Jennings, R. J., Bernstein, G. M., et al. 2016, AJ, 151, 39, doi: [10.3847/0004-6256/151/2/39](https://doi.org/10.3847/0004-6256/151/2/39)
- Gerdes, D. W., Sako, M., Hamilton, S., et al. 2017, ApJL, 839, L15, doi: [10.3847/2041-8213/aa64d8](https://doi.org/10.3847/2041-8213/aa64d8)
- Grav, T., Mainzer, A. K., Bauer, J., et al. 2011, ApJ, 742, 40, doi: [10.1088/0004-637X/742/1/40](https://doi.org/10.1088/0004-637X/742/1/40)
- Harris, C. R., Millman, K. J., van der Walt, S. J., et al. 2020, Nature, 585, 357, doi: [10.1038/s41586-020-2649-2](https://doi.org/10.1038/s41586-020-2649-2)
- Hendler, N. P., & Malhotra, R. 2020, PSJ, 1, 75, doi: [10.3847/PSJ/abbe25](https://doi.org/10.3847/PSJ/abbe25)
- Holmberg, J., Flynn, C., & Portinari, L. 2006, Monthly Notices of the Royal Astronomical Society, 367, 449, doi: [10.1111/j.1365-2966.2005.09832.x](https://doi.org/10.1111/j.1365-2966.2005.09832.x)
- Hunter, J. D. 2007, Computing in Science & Engineering, 9, 90, doi: [10.1109/MCSE.2007.55](https://doi.org/10.1109/MCSE.2007.55)
- Ivezić, Ž., Tabachnik, S., Rafikov, R., et al. 2001, AJ, 122, 2749, doi: [10.1086/323452](https://doi.org/10.1086/323452)
- Ivezić, Ž., Lupton, R. H., Jurić, M., et al. 2002, AJ, 124, 2943, doi: [10.1086/344077](https://doi.org/10.1086/344077)
- Khain, T., Becker, J. C., Lin, H. W., et al. 2020, AJ, 159, 133, doi: [10.3847/1538-3881/ab7002](https://doi.org/10.3847/1538-3881/ab7002)
- Levison, H. F., Olkin, C. B., Noll, K. S., et al. 2021, The Planetary Science Journal, 2, 171, doi: [10.3847/psj/abf840](https://doi.org/10.3847/psj/abf840)
- Lin, H. W., Gerdes, D. W., Hamilton, S. J., et al. 2019, Icarus, 321, 426, doi: [10.1016/j.icarus.2018.12.006](https://doi.org/10.1016/j.icarus.2018.12.006)
- Mainzer, A., Bauer, J., Grav, T., et al. 2011, ApJ, 731, 53, doi: [10.1088/0004-637X/731/1/53](https://doi.org/10.1088/0004-637X/731/1/53)
- Marzari, F., & Scholl, H. 1998, Icarus, 131, 41, doi: [10.1006/icar.1997.5841](https://doi.org/10.1006/icar.1997.5841)

- 531 McKinney, W., et al. 2010, in Proceedings of the 9th
532 Python in Science Conference, Vol. 445, Austin, TX,
533 51–56
- 534 Morbidelli, A., Levison, H. F., Bottke, W. F., Dones, L., &
535 Nesvorný, D. 2009, *Icarus*, 202, 310,
536 doi: [10.1016/j.icarus.2009.02.033](https://doi.org/10.1016/j.icarus.2009.02.033)
- 537 Morbidelli, A., Levison, H. F., Tsiganis, K., & Gomes, R.
538 2005, *Nature*, 435, 462, doi: [10.1038/nature03540](https://doi.org/10.1038/nature03540)
- 539 Mottola, S., Di Martino, M., Erikson, A., et al. 2011, *AJ*,
540 141, 170, doi: [10.1088/0004-6256/141/5/170](https://doi.org/10.1088/0004-6256/141/5/170)
- 541 Napier, K. 2020, *SpaceRocks*,
542 <https://github.com/kjnapier/spacerocks>
- 543 Nesvorný, D., Vokrouhlický, D., & Morbidelli, A. 2013, in
544 AAS/Division for Planetary Sciences Meeting Abstracts,
545 Vol. 45, AAS/Division for Planetary Sciences Meeting
546 Abstracts #45, 508.03
- 547 Roig, F., & Nesvorný, D. 2015, *AJ*, 150, 186,
548 doi: [10.1088/0004-6256/150/6/186](https://doi.org/10.1088/0004-6256/150/6/186)
- 549 Szabó, G. M., Ivezić, Ž., Jurić, M., & Lupton, R. 2007,
550 *MNRAS*, 377, 1393,
551 doi: [10.1111/j.1365-2966.2007.11687.x](https://doi.org/10.1111/j.1365-2966.2007.11687.x)
- 552 Uehata, K., Terai, T., Ohtsuki, K., & Yoshida, F. 2022, *AJ*,
553 163, 213, doi: [10.3847/1538-3881/ac5b6d](https://doi.org/10.3847/1538-3881/ac5b6d)
- 554 Virtanen, P., Gommers, R., Oliphant, T. E., et al. 2020,
555 *Nature Methods*, 17, 261, doi: [10.1038/s41592-019-0686-2](https://doi.org/10.1038/s41592-019-0686-2)
- 556 Walsh, K. J., Morbidelli, A., Raymond, S. N., O’Brien,
557 D. P., & Mandell, A. M. 2011, *Nature*, 475, 206,
558 doi: [10.1038/nature10201](https://doi.org/10.1038/nature10201)
- 559 Wong, I., & Brown, M. E. 2015, *AJ*, 150, 174,
560 doi: [10.1088/0004-6256/150/6/174](https://doi.org/10.1088/0004-6256/150/6/174)
- 561 —. 2016, *AJ*, 152, 90, doi: [10.3847/0004-6256/152/4/90](https://doi.org/10.3847/0004-6256/152/4/90)
- 562 Wong, I., Brown, M. E., Blacksberg, J., Ehlmann, B. L., &
563 Mahjoub, A. 2019, *AJ*, 157, 161,
564 doi: [10.3847/1538-3881/ab0e00](https://doi.org/10.3847/1538-3881/ab0e00)
- 565 Wong, I., Brown, M. E., & Emery, J. P. 2014, *AJ*, 148, 112,
566 doi: [10.1088/0004-6256/148/6/112](https://doi.org/10.1088/0004-6256/148/6/112)
- 567 —. 2017, *AJ*, 154, 104, doi: [10.3847/1538-3881/aa8406](https://doi.org/10.3847/1538-3881/aa8406)
- 568 Yoshida, F., & Nakamura, T. 2005, *AJ*, 130, 2900,
569 doi: [10.1086/497571](https://doi.org/10.1086/497571)
- 570 —. 2008, *PASJ*, 60, 297, doi: [10.1093/pasj/60.2.297](https://doi.org/10.1093/pasj/60.2.297)
- 571 Yoshida, F., & Terai, T. 2017, *AJ*, 154, 71,
572 doi: [10.3847/1538-3881/aa7d03](https://doi.org/10.3847/1538-3881/aa7d03)
- 573 Yoshida, F., Terai, T., Ito, T., et al. 2019,
574 *Planet. Space Sci.*, 169, 78, doi: [10.1016/j.pss.2019.02.003](https://doi.org/10.1016/j.pss.2019.02.003)